

# The chemistry of ions in the Orion Bar I. - CH<sup>+</sup>, SH<sup>+</sup> and CF<sup>+</sup>

## The effect of high electron density and vibrationally excited H<sub>2</sub> in a warm PDR surface

Z. Nagy<sup>1,2</sup>, F.F.S. Van der Tak<sup>2,1</sup>, V. Ossenkopf<sup>3</sup>, M. Gerin<sup>4</sup>, F. Le Petit<sup>5</sup>, J. Le Bourlot<sup>5</sup>, J. H. Black<sup>6</sup>, J. R. Goicoechea<sup>7</sup>, C. Joblin<sup>8,9</sup>, M. Röllig<sup>3</sup>, and E. A. Bergin<sup>10</sup>

<sup>1</sup> Kapteyn Astronomical Institute, PO Box 800, 9700 AV, Groningen, The Netherlands  
e-mail: nagy@astro.rug.nl

<sup>2</sup> SRON Netherlands Institute for Space Research, PO Box 800, 9700 AV, Groningen, The Netherlands

<sup>3</sup> I. Physikalisches Institut der Universität zu Köln, Zùlpicher Straße 77, 50937 Köln, Germany

<sup>4</sup> LERMA, UMR 8112 du CNRS, Observatoire de Paris, École Normale Supérieure, France

<sup>5</sup> Observatoire de Paris, LUTH and Université Denis Diderot, Place J. Janssen, 92190 Meudon, France

<sup>6</sup> Chalmers University of Technology, Department of Earth and Space Sciences, Onsala Space Observatory, 43992 Onsala, Sweden

<sup>7</sup> Centro de Astrobiología, CSIC-INTA, 28850 Madrid, Spain

<sup>8</sup> Université de Toulouse, UPS-OMP, IRAP, Toulouse, France

<sup>9</sup> CNRS, IRAP, 9 Av. colonel Roche, BP 44346, 31028 Toulouse Cedex 4, France

<sup>10</sup> Department of Astronomy, The University of Michigan, 500 Church Street, Ann Arbor, MI 48109-1042, USA

Received October 8, 2012; accepted December 12, 2012

### ABSTRACT

**Context.** The abundances of interstellar CH<sup>+</sup> and SH<sup>+</sup> are not well understood as their most likely formation channels are highly endothermic. Several mechanisms have been proposed to overcome the high activation barriers, including shocks, turbulence and H<sub>2</sub> vibrational excitation.

**Aims.** Using data from the Herschel Space Observatory, we study the formation of ions, in particular CH<sup>+</sup> and SH<sup>+</sup> in a typical high UV-illumination warm and dense photon-dominated region (PDR), the Orion Bar.

**Methods.** The HIFI instrument onboard Herschel provides velocity-resolved line profiles of CH<sup>+</sup> 1-0 and 2-1 and three hyperfine transitions of SH<sup>+</sup> 1<sub>2</sub> – 0<sub>1</sub>. The PACS instrument provides information on the excitation and spatial distribution of CH<sup>+</sup> by extending the observed CH<sup>+</sup> transitions up to  $J = 6 - 5$ . We compare the observed line intensities to the predictions of radiative transfer and PDR codes.

**Results.** All CH<sup>+</sup>, SH<sup>+</sup> and CF<sup>+</sup> lines analysed in this paper are seen in emission. The widths of the CH<sup>+</sup> 2-1 and 1-0 transitions are of  $\sim 5$  km s<sup>-1</sup>, significantly broader than the typical width of dense gas tracers in the Orion Bar ( $\sim 2-3$  km s<sup>-1</sup>) and are comparable to the width of tracers of the interclump medium such as C<sup>+</sup> and HF. The detected SH<sup>+</sup> transitions are narrower compared to CH<sup>+</sup> and have line widths of  $\sim 3$  km s<sup>-1</sup>, indicating that SH<sup>+</sup> emission mainly originates in denser condensations. Non-LTE radiative transfer models show that electron collisions affect the excitation of CH<sup>+</sup> and SH<sup>+</sup>, and that reactive collisions need to be taken into account to calculate the excitation of CH<sup>+</sup>. Comparison to PDR models shows that CH<sup>+</sup> and SH<sup>+</sup> are tracers of the warm surface region ( $A_V < 1.5$ ) of the PDR with temperatures between 500-1000 K. We have also detected the 5-4 transition of CF<sup>+</sup> at a width of  $\sim 1.9$  km s<sup>-1</sup>, consistent with the width of dense gas tracers. The intensity of the CF<sup>+</sup> 5-4 transition is consistent with previous observations of lower- $J$  transitions toward the Orion Bar.

**Conclusions.** An analytic approximation as well as a numerical comparison to PDR models indicate that the internal vibrational energy of H<sub>2</sub> can explain the formation of CH<sup>+</sup> for typical physical conditions in the Orion Bar near the ionization front. H<sub>2</sub> vibrational excitation is the most likely explanation of SH<sup>+</sup> formation as well. The abundance ratios of CH<sup>+</sup> and SH<sup>+</sup> trace the destruction paths of these ions, and through that, indirectly, the ratios of H, H<sub>2</sub> and electron abundances as a function of depth into the cloud.

**Key words.** ISM: molecules – ISM: individual objects: Orion Bar

## 1. Introduction

CH<sup>+</sup> is one of the first molecules that have been detected in the interstellar medium (Douglas & Herzberg 1941). Early studies of CH<sup>+</sup> found its abundance to be consistently larger than the predictions of steady-state chemical models in quiescent molecular clouds (e.g. Van Dishoeck & Black 1986). One of the possible formation routes is the endothermic reaction  $C^+ + H_2 + 0.41 \text{ eV} \rightarrow CH^+ + H$ . To reproduce the observed CH<sup>+</sup> abundances, several explanations have been proposed on

how to overcome the high activation barrier of the formation reaction. For low-density diffuse interstellar clouds, C-shocks (Pineau des Forêts et al. 1986) and turbulent dissipation (Godard et al. 2009) have been proposed and confirmed by Falgout et al. (2010a,b) and Godard et al. (2012). Alternatively, in denser regions with strong FUV radiation fields, the internal energy available in the vibrationally excited H<sub>2</sub> molecules has been proposed to help overcoming the large activation barrier (Sternberg & Dalgarno 1995, Agundez et al. 2010).

$\text{SH}^+$  has a similar chemistry to  $\text{CH}^+$ , having a formation route via  $\text{S}^+$  and  $\text{H}_2$ , however, this reaction is twice as endothermic as the  $\text{CH}^+$  formation reaction. After non-detections of  $\text{SH}^+$  in the UV domain in the spectra of nearby stars (Millar & Hobbs 1988, Magnani & Salzer 1991), the 526 GHz  $N_J = 1_2 - 0_1$  transition of  $\text{SH}^+$  has been detected in emission using Herschel toward the high-mass protostar W3 IRS 5 (Benz et al. 2010). The 526 GHz transition has also been detected in absorption in the diffuse interstellar medium towards various distant star-forming regions (Godard et al. 2012). The 683 GHz transition of  $\text{SH}^+$  has been detected in absorption towards Sgr B2(M) from the ground with the CHAMP+ receiver of APEX (Menten et al. 2011).

In this paper, we study the formation and excitation of  $\text{CH}^+$  and  $\text{SH}^+$  in a prototypical photon-dominated region (PDR), the Orion Bar. The Orion Bar is located at a distance of 414 pc (Menten et al. 2007). Its stratified structure has been a subject of many previous studies (such as Van der Wiel et al. 2009 and references therein). The mean density of the Orion Bar is about  $\geq 10^5 \text{ cm}^{-3}$ , the mean molecular gas temperature 85 K (Hogerheijde et al. 1995), and the impinging radiation field is  $(1 - 4) \times 10^4$  in Draine units (Draine field:  $\chi = 2.7 \times 10^{-3} \text{ erg s}^{-1} \text{ cm}^{-2}$  for the energy range between  $6 < h\nu < 13.6 \text{ eV}$ ; Draine 1978). Most of the low- $J$  molecular line emission originates in an interclump medium with a density between a few  $10^4$  and  $2 \times 10^5 \text{ cm}^{-3}$  (Simon et al. 1997). High-density tracers such as HCN and  $\text{H}^{13}\text{CN}$  originate in dense clumps, as confirmed by interferometric observations (Young Owl et al. 2000). The density of the clumps is in range between  $1.5 \times 10^6$  and  $6 \times 10^6 \text{ cm}^{-3}$  (Lis & Schilke 2003). Apart from the large clumps detected in e.g.  $\text{H}^{13}\text{CN}$  deep inside the Bar, small, warm ( $T_{\text{kin}} \sim 160 - 220 \text{ K}$ ) and dense ( $n_{\text{H}} \sim 10^{6-7} \text{ cm}^{-3}$ ) condensations have been suggested to explain the excited OH emission at the PDR surface (Goicoechea et al. 2011).

This paper aims to characterize the medium where ions such as  $\text{CH}^+$  and  $\text{SH}^+$  form as well as to distinguish between the explanations on how to overcome the high activation barriers of the formation reaction in a warm and dense PDR. We also report the detection of the  $\text{CF}^+$  5-4 transition. We will address another ion,  $\text{OH}^+$  in a separate paper (Van der Tak & Nagy et al., in prep).

## 2. Observations and Data reduction

The  $\text{CO}^+$  peak ( $\alpha_{\text{J2000}} = 05^{\text{h}}35^{\text{m}}20.6^{\text{s}}$ ,  $\delta_{\text{J2000}} = -05^{\circ}25'14''$ ) in the Orion Bar (Störzer et al. 1995) has been observed in every HIFI band as a spectral scan as part of the HEXOS (Herschel observations of EXtra-Ordinary Sources) guaranteed-time key program (Bergin et al. 2010) for the HIFI instrument of the Herschel Space Observatory. The data were reduced using HIPE (Ott et al. 2010) pipeline version 6.0. The velocity calibration of HIFI data is accurate to  $\sim 0.5 \text{ km s}^{-1}$  or better. The sideband deconvolution was done using the *doDeconvolution* task in HIPE. In this paper we use the HIFI bands 1a, 1b, 2a and 3a from the HEXOS spectral line survey. These observations were carried out in 2011 March and April in load chop mode with a redundancy of 4 and have total integration times of 2.4 h, 2.2 h, 3.1 h and 1.3 h, respectively. The WBS (Wide-Band Spectrometer) backend was used which covers 4 GHz bandwidth in four 1140 MHz subbands at 1.1 MHz resolution.

In addition to HIFI spectral scans observed as a part of the HEXOS key program, the  $\text{CH}^+$  2-1 transition has been observed as a deep integration in a spectral scan in band 6b, with a total integration time of 11.7 h and a redundancy 4 in dual beam switch (DBS) mode. Both WBS and HRS (High Resolution Spectrometer) backends were used. It has been reduced using HIPE pipeline version 8.0.

Besides the HIFI data, we use observations of the  $\text{CH}^+$  3-2, 4-3, 5-4 and 6-5 transitions from the PACS spectrometer (Poglitsch et al. 2010) onboard Herschel. The PACS observations were carried out on September 2010 and consist of two spectral scans in Range Spectroscopy mode with 5 range repetitions each (Joblin et al. 2012, in prep). The PACS spectrometer provides 25 spectra over a  $47'' \times 47''$  field-of-view resolved in  $5 \times 5$  spatial pixels (“spaxels”), each with a size of  $\sim 9.4''$  on the sky. The measured width of the spectrometer point spread function (PSF) is relatively constant at  $\lambda \lesssim 100 \mu\text{m}$  but it significantly increases above the spaxel size for longer wavelengths. The resolving power varies between  $\lambda/\Delta\lambda \sim 1000$  (R1 grating order) and  $\sim 5000$  (B3A grating order). The central spaxel was centered at the same HIFI survey position. Observations were carried in the “chop-nodded” mode with the largest chopper throw of 6 arcmin. The total integration time was 3.2 h for the 1342204117 observation (B2B and R1) and 2.7 h for the 1342204118 observation (B3A). PACS data were processed using HIPE 6.0.3.

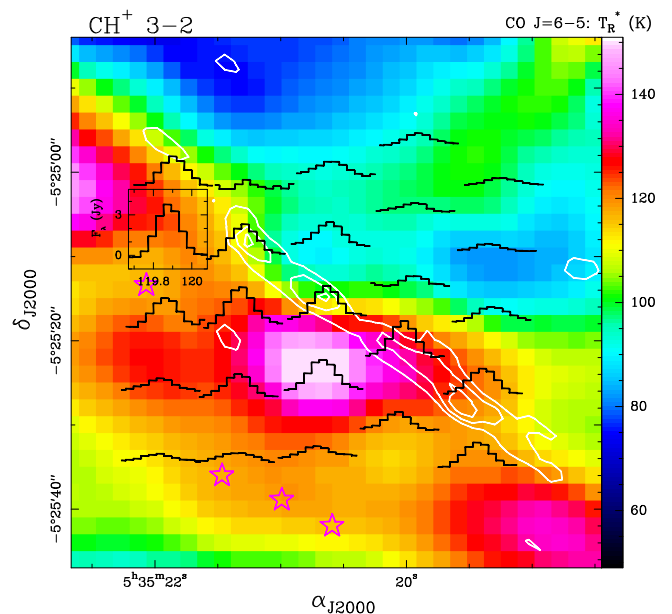


**Fig. 1.** PACS  $\text{CH}^+$  3-2 lines (black) -centered on the  $\text{CO}^+$  peak- overlaid on the distribution of the  $\text{CO } J = 6 - 5$  peak brightness temperature (colour image) observed with the CSO telescope at  $\sim 11''$  resolution (Lis et al. 1998). The PACS line intensity distributions are shown in units of Jy/spaxel as a function of wavelength in  $\mu\text{m}$  and are not velocity resolved. White contours show the brightest regions of  $\text{H}_2^+ v = 1 - 0$  S (1) emission (Walmsley et al. 2000). Lower intensity  $\text{H}_2^+$  extended emission is present in the entire field (Van der Werf et al. 1996). Violet stars show the position of the  $\text{H}^{13}\text{CN } J = 1 - 0$  clumps deeper inside the Bar (Lis & Schilke 2003).

Table 1 shows the spectroscopic and observational parameters of the transitions used in this paper. The rest frequencies are based on the CDMS database (Müller et al. 2005). In particular, the frequencies of the  $\text{CH}^+$  1-0 and 2-1 and  $^{13}\text{CH}^+$  1-0 transitions are based on Müller (2010).

Table 2 includes the observed line parameters for our line sample observed with HIFI, which have been corrected for main beam efficiencies based on Roelfsema et al. (2012). In the case of the detected HIFI transitions we use the average of H and V polarizations. The detected lines show similar line profiles in both polarizations. The intensity difference between the polarizations is 12% for  $\text{CH}^+ J = 1 - 0$ , 8% for  $\text{CH}^+ J = 2 - 1$ ,  $\sim 20\%$

for SH<sup>+</sup>  $N_J = 1_2 - 0_1$  and  $\sim 30\%$  for CF<sup>+</sup> 5-4. To compare the line intensities of the transitions detected with HIFI with different beam sizes, we convert all the observed line intensities to a common,  $\sim 47''$  resolution. We derive conversion factors between the original beam sizes and  $\sim 47''$  based on the integrated intensity map of the HCN 4-3 transition from the JCMT Spectral Legacy Survey (Van der Wiel et al. 2009). For this, we assume the intensity distribution of the HCN 4-3 transition to trace the spatial structure of the Orion Bar. For the PACS data (Table 2), due to uncertainties in the PSF-correction, we use the mean value of the intensity measured at the central spaxel ( $I_{\text{central}}$ ) and that corresponding to the value integrated over  $3 \times 3$  spaxels around center ( $I_{3 \times 3}$ ). The corresponding error bars are the difference between  $I_{\text{central}}$  and  $I_{3 \times 3}$ . This method provides a correct agreement between SPIRE and HIFI data for CO lines (Joblin et al. 2012, in prep). The large (40%) error bar corresponding to the intensity of the 5-4 transition is due to the presence of oscillations (fringes) in this range. Due to a lower band intensity and a significant noise level, only  $I_{3 \times 3}$  was measured for the intensity of the 6-5 transition.  $I_{\text{central}}$  was then estimated using a standard error value.

### 3. Results

#### 3.1. The detected CH<sup>+</sup>, SH<sup>+</sup> and CF<sup>+</sup> transitions

Figure 2 shows the velocity-resolved CH<sup>+</sup> transitions, that are detected with significantly broad lines ( $\sim 5 \text{ km s}^{-1}$ ) compared to the line width of dense gas tracers in the Orion Bar ( $\sim 2-3 \text{ km s}^{-1}$ , Hogerheijde et al. 1995 and an example of the CO 16-15 transition on Figure 2). The line width of the CH<sup>+</sup> 2-1 and 1-0 transitions is not only significantly larger than the width of dense gas tracers, but of species that trace a similar region as CH<sup>+</sup>, such as CO<sup>+</sup> (Störzer et al. 1995, Fuente et al. 2003). The  $5 \text{ km s}^{-1}$  is rather comparable to the width of tracers of the interclump medium, such as C<sup>+</sup> ( $\Delta v \sim 3.8 \text{ km s}^{-1}$ , also shown on Fig. 2) and HF ( $\Delta v \sim 4.9 \text{ km s}^{-1}$ , Van der Tak et al. 2012).

Other, non velocity-resolved transitions from PACS, such as the  $J=3-2$  transition (Fig. 1) show extended emission detected over all PACS spaxels, decreasing with distance from the ionization front. The maximum CH<sup>+</sup> 3-2 emission is seen further into the nearly edge-on PDR compared to the peak H<sub>2</sub>  $v=1-0$  emission (Figure 1). As CH<sup>+</sup> forms via a reaction between C<sup>+</sup> and H<sub>2</sub>, we compare the CH<sup>+</sup> 3-2 intensity distribution to C<sup>+</sup> emission from Figure 4. in Ossenkopf et al. (2012). The C<sup>+</sup> peak matches the CH<sup>+</sup> peak within the HIFI beam. This indicates that CH<sup>+</sup> formation is rather limited by the C<sup>+</sup> abundance than by the H<sub>2</sub> excitation that is traced by the H<sub>2</sub>  $v = 1 - 0$  S(1) emission observed by Walmsley et al. (2000).

Figure 3 shows a tentative detection of the <sup>13</sup>CH<sup>+</sup>  $J = 1-0$  in V-polarization. If it was a real detection, the observed <sup>12</sup>CH<sup>+</sup>/<sup>13</sup>CH<sup>+</sup> line ratio of  $\sim 40$  would indicate an optical depth of the <sup>12</sup>CH<sup>+</sup> line of  $\sim$ unity, assuming that the <sup>13</sup>CH<sup>+</sup> emission is optically thin. However, this seems unlikely, since a <sup>12</sup>CH<sup>+</sup> optical depth of  $\sim 1$  at a temperature  $> 100 \text{ K}$  (discussed in the following sections e.g. Sect. 3.2) is inconsistent with the observed <sup>12</sup>CH<sup>+</sup> line intensity. Further, deeper observations are needed to confirm the detection of <sup>13</sup>CH<sup>+</sup>.

Figure 4 shows three hyperfine components of the  $N_J = 1_2 - 0_1$  transition of SH<sup>+</sup> ( $F = 3/2 - 1/2$ ,  $F = 5/2 - 3/2$  and  $F = 3/2 - 3/2$ ). The SH<sup>+</sup>  $F=3/2-3/2$  transition is only detected in V-polarization. The line width of the detected SH<sup>+</sup> transitions ( $3.0 \text{ km s}^{-1}$ ) is narrower than those of CH<sup>+</sup> and are consistent with

the width of dense-gas tracers in the Orion Bar, suggesting that it does not originate in the same gas component as CH<sup>+</sup>.

We have also detected the CF<sup>+</sup> 5-4 transition, for the first time, with a line width of  $\sim 2 \text{ km s}^{-1}$  (Fig. 5). The 3-2, 2-1 and 1-0 transitions of CF<sup>+</sup> have previously been detected toward the Orion Bar from the ground by Neufeld et al. (2006) with beam sizes of HPBW=24'', 12'' and 21'' (respectively). The velocity and the width of the 5-4 transition is consistent with the parameters reported for the other detected transitions by Neufeld et al. (2006). One of the positions covered by Neufeld et al. (2006), ('CO position', 05<sup>h</sup>35<sup>m</sup>22.8<sup>s</sup>, -5°25'01'') is close ( $\Delta \text{RA} \sim 30''$ ,  $\Delta \text{Dec} \sim 13''$ ) to our observed position which is within the beam of HIFI at the frequency of the 5-4 transition ( $\sim 44.2''$ ). Assuming uniform beam-filling, a single excitation temperature of all four levels and optically thin lines, the measured line intensity is consistent with those detected by Neufeld et al. (2006) (Fig. 6) and implies a column density of  $\sim 2.1 \times 10^{12} \text{ cm}^{-2}$  and a rotation temperature of  $\sim 32 \text{ K}$ .

We derive upper limits for other, non-detected CF<sup>+</sup> and SH<sup>+</sup> transitions. We estimate rms noise levels in the averaged spectrum of H and V polarizations.  $3\sigma$  upper limits on the integrated line intensities are estimated using (e.g. Coutens et al. 2012):

$$I(3\sigma) [\text{K km s}^{-1}] = 3 \text{ rms } \sqrt{2} dv \text{ FWHM}$$

where  $dv$  is the channel width in  $\text{km s}^{-1}$  and the rms noise level is derived in a velocity range of  $\pm 5 \text{ km s}^{-1}$  around the expected velocity. We use an FWHM of  $1.9 \text{ km s}^{-1}$  for the <sup>13</sup>CF<sup>+</sup> 5-4 (488664.3 MHz) and the CF<sup>+</sup> 6-5 (615365.6 MHz) upper limits, and FWHM=3  $\text{km s}^{-1}$  for SH<sup>+</sup>  $N_J = 1_1 - 0_1$  ( $\sim 683 \text{ GHz}$ ). The derived  $3\sigma$  upper limits are listed in Table 2.

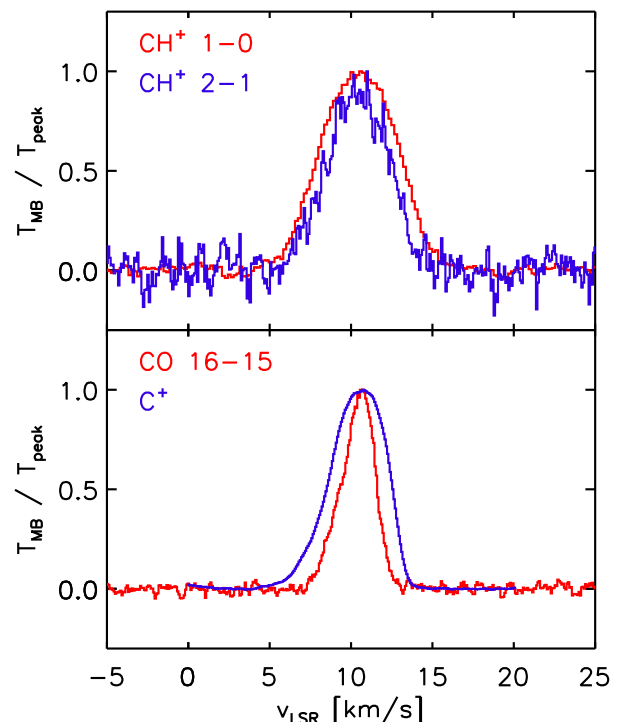


Fig. 2. Top panel: The line profiles of the CH<sup>+</sup> 2-1 and 1-0 transitions corresponding to the average of H and V polarizations observed with Herschel/HIFI toward the CO<sup>+</sup> peak in the Orion Bar. Bottom panel: Line profiles of C<sup>+</sup> and CO 16-15 for a comparison, observed with Herschel/HIFI toward the CO<sup>+</sup> peak in the Orion Bar.

**Table 1.** Spectroscopic and observational parameters of the transitions used in this paper.

Transition	Frequency (MHz)	$E_{\text{up}}$ (K)	A ( $\text{s}^{-1}$ )	instrument/band	beam-size ( $''$ )	$\eta_{\text{mb}}$
$\text{CH}^+$ 1–0	835137.5	40.1	$6.36 \times 10^{-3}$	HIFI, band 3a	26.5	0.75
$\text{CH}^+$ 2–1	1669281.3	120.2	$6.10 \times 10^{-2}$	HIFI, band 6b	15.0	0.72
$\text{CH}^+$ 3–2	2501440.5	240.2	$2.20 \times 10^{-1}$	PACS	9.4 <sup>1</sup>	
$\text{CH}^+$ 4–3	3330629.7	400.1	$5.38 \times 10^{-1}$	PACS	9.4 <sup>1</sup>	
$\text{CH}^+$ 5–4	4155872.0	599.5	1.07	PACS	9.4 <sup>1</sup>	
$\text{CH}^+$ 6–5	4976201.4	838.3	1.86	PACS	9.4 <sup>1</sup>	
$^{13}\text{CH}^+$ 1–0	830216.1	39.9	$5.83 \times 10^{-3}$	HIFI, band 3a	26.5	0.75
$\text{SH}^+ N_J = 1_2 - 0_1, F = 3/2 - 1/2$	526038.7	25.3	$7.99 \times 10^{-4}$	HIFI, band 1a	44.2	0.76
$\text{SH}^+ N_J = 1_2 - 0_1, F = 5/2 - 3/2$	526047.9	25.3	$9.59 \times 10^{-4}$	HIFI, band 1a	44.2	0.76
$\text{SH}^+ N_J = 1_2 - 0_1, F = 3/2 - 3/2$	526124.9	25.3	$1.60 \times 10^{-4}$	HIFI, band 1a	44.2	0.76
$\text{SH}^+ N_J = 1_1 - 0_1, F = 3/2 - 1/2$	683336.1	32.8	$2.90 \times 10^{-4}$	HIFI, band 2a	33.2	0.75
$\text{SH}^+ N_J = 1_1 - 0_1, F = 1/2 - 1/2$	683362.0	32.8	$1.16 \times 10^{-3}$	HIFI, band 2a	33.2	0.75
$\text{SH}^+ N_J = 1_1 - 0_1, F = 3/2 - 3/2$	683422.3	32.8	$1.45 \times 10^{-3}$	HIFI, band 2a	33.2	0.75
$\text{SH}^+ N_J = 1_1 - 0_1, F = 1/2 - 3/2$	683448.2	32.8	$5.79 \times 10^{-4}$	HIFI, band 2a	33.2	0.75
$\text{CF}^+$ 5–4	512846.5	73.8	$8.21 \times 10^{-4}$	HIFI, band 1a	44.2	0.76
$\text{CF}^+$ 6–5	615365.6	103.4	$1.44 \times 10^{-3}$	HIFI, band 1b	44.2	0.76
$^{13}\text{CF}^+$ 5–4	488664.3	70.0	$7.10 \times 10^{-4}$	HIFI, band 1a	44.2	0.76

<sup>1</sup> The size of one PACS spaxel.**Table 2.** The detected  $\text{CH}^+$ ,  $\text{SH}^+$  and  $\text{CF}^+$  transitions and the gaussian fit parameters for the velocity-resolved transitions observed with HIFI and PACS and upper limits for non-detections of other  $\text{CF}^+$  and  $\text{SH}^+$  transitions. The  $\text{CH}^+$   $J = 3 - 2, 4 - 3, 5 - 4$  and  $6 - 5$  transitions are spectrally unresolved from PACS. The parameters from HIFI are based on the average spectrum of H and V polarizations, unless otherwise specified.

Line	$\int T_{\text{MB}} dV$ (K km s <sup>-1</sup> )	$V_{\text{LSR}}$ (km s <sup>-1</sup> )	$\Delta V$ (km s <sup>-1</sup> )	$T_{\text{peak}}$ (K)	rms( $T_{\text{MB}}$ ) (K)
$\text{CH}^+$ 1–0	24.9±0.20	10.5±0.02	5.46±0.04	4.28±0.15	0.12
$\text{CH}^+$ 2–1	10.6±0.20	10.4±0.05	4.57±0.11	2.18±0.22	0.23
$\text{CH}^+$ 3–2	2.19±0.31				
$\text{CH}^+$ 4–3	1.01±0.19				
$\text{CH}^+$ 5–4	0.42±0.15				
$\text{CH}^+$ 6–5	0.17±0.06				
$^{13}\text{CH}^+$ 1–0 <sup>1</sup>	0.46±0.11	11.39±0.15	1.30±0.34	0.34±0.10	0.15
$\text{SH}^+ N_J = 1_2 - 0_1 F = 3/2 - 1/2$	0.34±0.02	10.92±0.09	3.00 <sup>2</sup>	0.11±0.02	0.02
$\text{SH}^+ N_J = 1_2 - 0_1 F = 5/2 - 3/2$	0.57±0.02	10.84±0.06	3.00 <sup>2</sup>	0.18±0.02	0.02
$\text{SH}^+ N_J = 1_2 - 0_1 F = 3/2 - 3/2$	0.14±0.02	10.34±0.24	3.00 <sup>2</sup>	0.04±0.01	0.02
$\text{SH}^+ N_J = 1_1 - 0_1 F = 3/2 - 1/2$	≤0.18			≤0.15 <sup>3</sup>	
$\text{SH}^+ N_J = 1_1 - 0_1 F = 1/2 - 1/2$	≤0.11			≤0.09 <sup>3</sup>	
$\text{SH}^+ N_J = 1_1 - 0_1 F = 3/2 - 3/2$	≤0.13			≤0.12 <sup>3</sup>	
$\text{SH}^+ N_J = 1_1 - 0_1 F = 1/2 - 3/2$	≤0.11			≤0.09 <sup>3</sup>	
$\text{CF}^+$ 5–4	0.20±0.02	11.13±0.11	1.96±0.21	0.10±0.01	0.02
$\text{CF}^+$ 6–5	≤0.08			≤0.08 <sup>3</sup>	
$^{13}\text{CF}^+$ 5–4	≤0.05			≤0.05 <sup>3</sup>	

<sup>1</sup> Based on V-polarization data only.<sup>2</sup> Fixed parameter in the fit.<sup>3</sup> 3×rms noise level.

### 3.2. Physical conditions traced by $\text{CH}^+$ and $\text{SH}^+$

To estimate molecular column densities, we use the non-LTE radiative transfer code Radex (Van der Tak et al. 2007). We use  $\text{H}_2$  as a collision partner for the excitation of  $\text{CH}^+$ , as we expect a significant fraction of hydrogen to be in a molecular form at the observed position. Rates for inelastic collisions between  $\text{CH}^+$  and H are not available, but are expected to be of the same order of magnitude as the rates for inelastic collisions between  $\text{CH}^+$  and  $\text{H}_2$ . If most H is in an atomic state, the density used as an in-

put parameter is then the sum of  $n(\text{H})$  and  $n(\text{H}_2)$ . We also include excitation via inelastic collisions between  $\text{CH}^+$  and electrons, as the importance of excitation by electrons for HF has been recently demonstrated by Van der Tak et al. (2012). We apply an electron density of  $\sim 10 \text{ cm}^{-3}$ . This is justified, if we assume that the electron abundance is determined by the abundance of  $\text{C}^+$ . The column density of  $\text{C}^+$  is of order  $10^{18} \text{ cm}^{-2}$  (Ossenkopf et al. 2012) and the  $\text{H}_2$  column density is of order  $10^{22} \text{ cm}^{-2}$  (e.g. Habart et al. 2010, Van der Wiel et al. 2009). This implies an



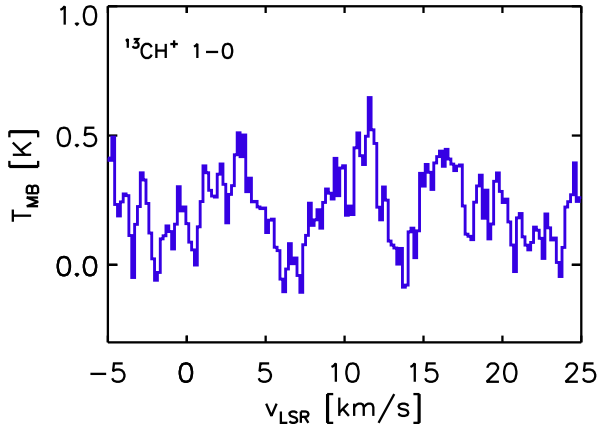


**Fig. 3.** The line profile of the  $^{13}\text{CH}^+$  1–0 transition observed with Herschel/HIFI in V polarization toward the CO<sup>+</sup> peak in the Orion Bar.

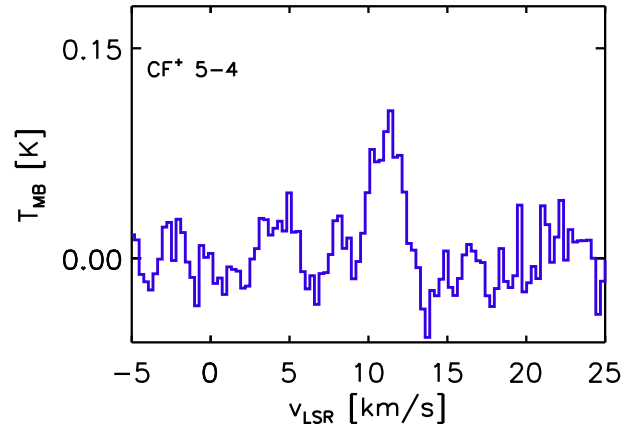


**Fig. 5.** The line profile of the CF<sup>+</sup> 5–4 transition corresponding to the average of H and V polarizations observed with Herschel/HIFI toward the CO<sup>+</sup> peak in the Orion Bar.

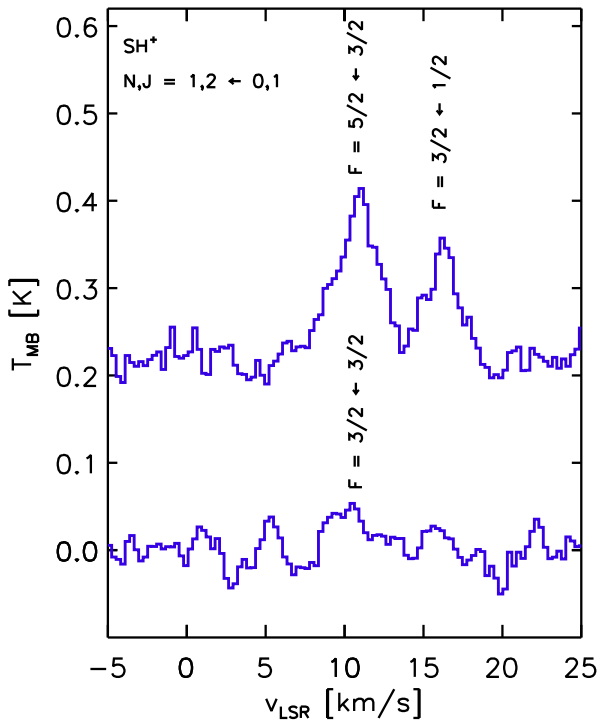


**Fig. 4.** The line profiles of the three hyperfine transitions of SH<sup>+</sup>  $N_J = 1_2 - 0_1$  observed with Herschel/HIFI corresponding to the average of H and V polarizations toward the CO<sup>+</sup> peak in the Orion Bar.

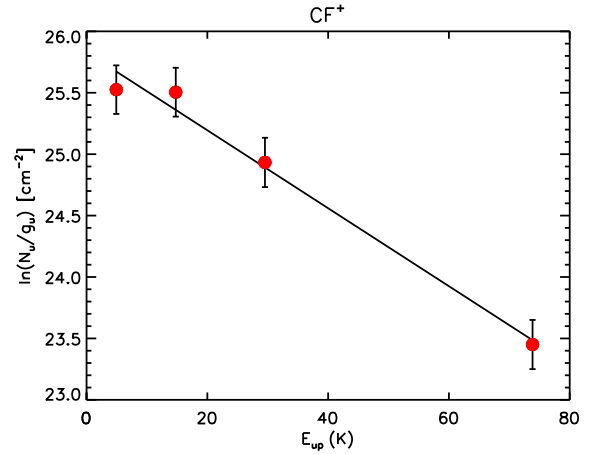


**Fig. 6.** Rotation diagram of CF<sup>+</sup> including the transitions detected by Neufeld et al. (2006).

electron abundance of  $10^{-4}$ , and using  $n(\text{H}_2) = 10^5 \text{ cm}^{-3}$ , an electron density of  $10 \text{ cm}^{-3}$ . In the following, we consider both H<sub>2</sub> and electron collisions to probe the excitation of CH<sup>+</sup> and SH<sup>+</sup>.

For CH<sup>+</sup>, our calculations are based on collision rates from Turpin et al. (2010), for temperatures in the range between 10 K and 200 K, covering transitions up to the 5–4 transition ( $E_{\text{up}} = 599.5 \text{ K}$ ). These rates have been scaled from CH<sup>+</sup>–He to CH<sup>+</sup>–H<sub>2</sub> based on Schöier et al. (2005). For electron collisions, we use collision rates from Lim et al. (1999), that are available for temperatures between 100–15000 K.

Collisions of H<sub>2</sub> and electrons are not always inelastic, but may also lead to a chemical reaction. In the case of CH<sup>+</sup>, this is important to take into account, since the collision rates with H<sub>2</sub> and electrons are comparable to the chemical reaction rates for CH<sup>+</sup> with H<sub>2</sub> and electrons. For example, for CH<sup>+</sup>–e<sup>−</sup>, the chemical reaction rate is  $9 \times 10^{-8} \text{ cm}^3 \text{ s}^{-1}$  for the destruction (Woodall et al. 2007) and is  $6.4 \times 10^{-7} \text{ cm}^3 \text{ s}^{-1}$  for the excitation of the  $J = 1 - 0$  transition at 1000 K. For CH<sup>+</sup>–H<sub>2</sub>, the destruction rate is  $1.2 \times 10^{-9} \text{ cm}^3 \text{ s}^{-1}$  (Woodall et al. 2007) and an excitation rate is  $1.1 \times 10^{-10} \text{ cm}^3 \text{ s}^{-1}$  for the  $J = 1 - 0$  transition at 100 K. Therefore, we consider the chemical formation and destruction rates in the statistical equilibrium calculation (e.g. Van der Tak et al. 2007). The statistical equilibrium for states  $i = 1 - N$  of energy  $E_i$  that is solved in the RADEX code is given by the time-independent rate equations:

$$\frac{dn_i}{dt} = \sum_{j \neq i} n_j P_{ji} - n_i \sum_{j \neq i} P_{ij} = \mathcal{F}_i - n_i \mathcal{D}_i \quad \text{cm}^{-3} \text{ s}^{-1}$$

where

$$\begin{aligned} P_{ij} &= A_{ij} + B_{ij} \bar{J} + C_{ij} \quad (E_i > E_j) \\ &= B_{ij} \bar{J} + C_{ij} \quad (E_i < E_j) \end{aligned}$$

and  $A_{ij}$  and  $B_{ij}$  are the Einstein coefficients,  $\bar{J}$  is the mean intensity at the frequency of transition  $i \rightarrow j$ ,  $C_{ij}$  is the sum over all collision partners of the rates of inelastic, collision-induced transitions  $i \rightarrow j$ ,  $n_i$  is the number density ( $\text{cm}^{-3}$ ) of molecules in level  $i$ , and  $\mathcal{D}_i$  is the rate of destruction of the molecule in level  $i$ . When detailed knowledge of the state-specific formation process is lacking, the formation rate into level  $i$  is expressed as a Boltzmann distribution over all states at an effective formation temperature  $T_f$ ,

$$\mathcal{F}_i \propto g_i \exp(-E_i/kT_f)$$

where  $g_i$  is the statistical weight of level  $i$ . When the destruction rate can be estimated, as for  $\text{CH}^+$  here, then the total formation rate is normalized so that the total number density of molecules is consistent with its column density and the density of hydrogen in steady state.

We assume that there is a balance between the formation and destruction of  $\text{CH}^+$ . To simulate the chemical pumping effect described above, i.e. the effect of destruction and subsequent formation of  $\text{CH}^+$  in excited levels, we add an artificial level to the  $\text{CH}^+$  level system, representing the dissociated state, that is populated with a rate equivalent to the reaction rate of  $\text{CH}^+-\text{H}_2$  and  $\text{CH}^+-\text{e}^-$  (Woodall et al. 2007). On the formation of  $\text{CH}^+$  through the reaction of  $\text{C}^+$  with vibrationally excited  $\text{H}_2$ , the re-population from the dissociated level follows a Boltzmann distribution with a formation temperature of  $T_f = 9920 \text{ K} - 4560 \text{ K} = 5360 \text{ K}$ , where 4560 K is the required energy input for the endothermic  $\text{CH}^+$  production and 9920 K is the average energy of the vibrationally excited  $\text{H}_2$  levels, following the 2-level approximation introduced by Röllig et al. (2006) where the full 15-level system was replaced by the energetically equivalent 2-level system that provides the same total vibrational heating.

Figure 7 shows the intensity predictions of two Radex models with parameters in the range that can be expected for the Orion Bar. The errorbars correspond to 10% calibration error and 10% error from obtaining integrated intensities by gaussian fitting for the transitions observed with HIFI. The error bars corresponding to the PACS data are dominated by uncertainty in the PSF correction and are estimated as explained in Section 2. Both electron collisions and  $\text{H}_2$  collisions suggest a kinetic temperature well above the average value (85 K) inferred for the interclump medium in the Orion Bar. Taking formation pumping and collisional excitation into account, as described above, we find reasonable fits to the observed line intensity distribution up to the 5-4 transition (the energy range for which the collision rates are available) with  $N(\text{CH}^+) = 9 \times 10^{14} \text{ cm}^{-2}$ ,  $T_{\text{kin}} = 500 \text{ K}$  and  $n(\text{H}_2) = 10^5 \text{ cm}^{-3}$ . The intensity of the 5-4 transition can be better reproduced with a kinetic temperature of  $T_{\text{kin}} = 1000 \text{ K}$ . Temperatures between 500 K and 1000 K are expected near the edge of the cloud, where the observations used in this paper have been taken. Including electron collisions, assuming an electron density of  $n_e = 10 \text{ cm}^{-3}$ , electron collisions mostly affect the two lowest- $J$  transitions for  $T_{\text{kin}} = 500 \text{ K}$  with an 10-13% increase in the intensities.

In the case of  $\text{SH}^+$ , calculations for collisions with  $\text{H}_2$  do not exist, so we use scaled radiative rates (J. Black, priv. comm.) for a temperature range of 10-5000 K. We also use collision rates for electron-impact collisions, calculated in the Coulomb-Born approximation (J. Black, priv. comm.), for a temperature range of 10-1000 K. Figure 8 shows the best fit models over-plotted on

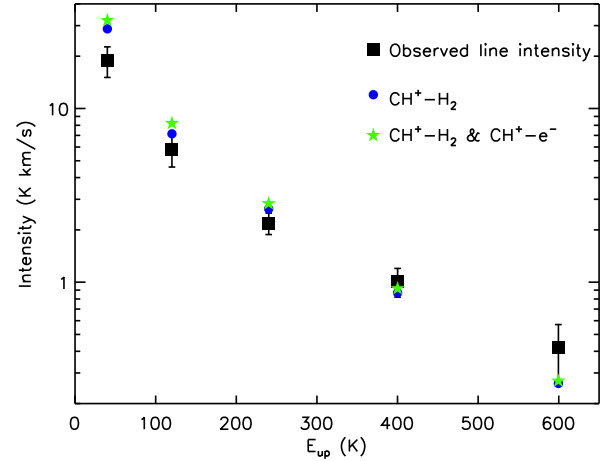


**Fig. 7.** The output of the Radex models corresponding to a model with  $N(\text{CH}^+) = 9 \times 10^{14} \text{ cm}^{-2}$ ,  $n(\text{H}_2) = 10^5 \text{ cm}^{-3}$ ,  $n(\text{e}^-) = 10 \text{ cm}^{-3}$ ,  $T_{\text{kin}} = 500 \text{ K}$ . The blue symbols correspond to a model with excitation via collisions with  $\text{H}_2$  and the green symbols correspond to a model with excitation via  $\text{H}_2$  and electron collisions.

the observed line intensities. The error bars correspond to 20% of the observed line intensities, including calibration error and the error introduced by the estimation of the integrated intensities using a gaussian fit. We consider lower kinetic temperatures and higher volume densities than in the case of  $\text{CH}^+$ , given that the line width suggests an origin from denser material. At the position of the  $\text{CO}^+$  peak, warm ( $T_{\text{kin}} \sim 160 - 220 \text{ K}$ ) and dense ( $10^{6-7} \text{ cm}^{-3}$ ) condensations have been suggested to explain the OH emission. Using  $\text{SH}^+-\text{H}_2$  collisions, a model with  $10^6 \text{ cm}^{-3}$ ,  $T_{\text{kin}} = 200 \text{ K}$  and  $N(\text{SH}^+) = 10^{13} \text{ cm}^{-2}$  gives a reasonable fit to the observed line intensities (Fig. 8). On Figure 8 we show a model with the same parameters, that includes electron collisions, assuming an electron density of  $n_e = 10 \text{ cm}^{-3}$ . In both of these models the excitation temperatures are low (8.3-10.4 K) and the lines are optically thin ( $\tau \sim 0.02 - 0.2$ ).

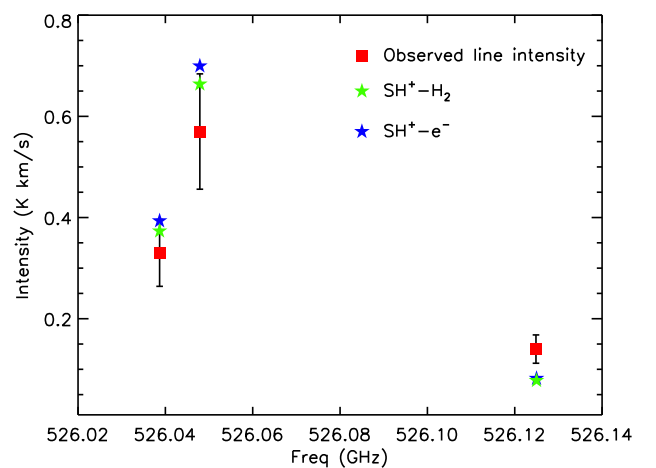


**Fig. 8.** The output of the Radex models for  $\text{H}_2$  and electron collisions compared to the observed line intensities of  $\text{SH}^+$  for a model with  $N(\text{SH}^+) = 10^{13} \text{ cm}^{-2}$ ,  $n(\text{H}_2) = 10^6 \text{ cm}^{-3}$ ,  $n(\text{e}^-) = 10 \text{ cm}^{-3}$  and  $T_{\text{kin}} = 200 \text{ K}$ .

#### 4. The formation of CH<sup>+</sup> and SH<sup>+</sup> via H<sub>2</sub> vibrational excitation

In this section, we investigate the role of H<sub>2</sub> vibrational excitation for the formation of CH<sup>+</sup> and SH<sup>+</sup>. We discuss alternative explanations in section 6.

##### 4.1. Estimate based on an analytic approximation

Testing if H<sub>2</sub> vibrational excitation can drive CH<sup>+</sup> and SH<sup>+</sup> formation in an environment with a given radiation field and physical parameters requires a detailed modeling with a PDR code, with information on the chemical network and physical processes that affect the level populations of vibrationally excited H<sub>2</sub>. A first indication can also be given using a simple analytic method to describe H<sub>2</sub> vibrational heating with a two level approximation (Röllig et al. 2006). The H<sub>2</sub> vibrational heating rate can be computed among all 15 vibrational levels in the ground electronic state (but neglecting the rotational structure) based on Equation C.2 in Röllig et al. (2006). A two-level system can be defined, that results in the same vibrational heating rate as the full, 15-level system (Equation C.3, Röllig et al. 2006). The vibrationally excited 'virtual' level has an upper level energy of  $\Delta E_{\text{eff}} = 9920$  K. The total rate for populating this vibrationally excited level:  $k_{0,1} = P_1 \chi$ , where  $\chi$  is the radiation field in Draine units (Draine 1978) and  $P_1 = 6.9 \times 10^{-10} \text{ s}^{-1}$  is the formation rate of vibrationally excited H<sub>2</sub> for the defined level for a radiation field of  $\chi = 1$ . The de-excitation of this vibrationally excited level is via spontaneous emission, dissociation by the UV radiation field and by collisional de-excitation. The coefficient for spontaneous decay is  $A_{\text{eff}} = 1.9 \times 10^{-6} \text{ s}^{-1}$ . The collisional de-excitation scales as  $n_{\text{gas}} \gamma_{\text{eff}}$ , with a rate coefficient of  $\gamma_{\text{eff}} = 5.4 \times 10^{-13} \sqrt{T} \text{ s}^{-1} \text{ cm}^{-3}$ . The dissociation rate is  $\chi \times D_{\text{eff}}$ , where  $D_{\text{eff}} = 4.7 \times 10^{-10} \text{ s}^{-1}$ . These effective coefficients ( $A_{\text{eff}}$ ,  $\gamma_{\text{eff}}$  and  $D_{\text{eff}}$ ) for the defined 2-level system as well as the energy of the defined vibrationally excited level ( $\Delta E_{\text{eff}}$ ) are obtained by considering different asymptotic values of the density  $n$  and the radiation field  $\chi$ . By neglecting dissociation, the population of the vibrationally excited level is dependent on the formation rate of vibrationally excited H<sub>2</sub> as well as on the spontaneous decay and collisional de-excitation rates. Calculating with  $n_{\text{gas}} = 10^5 \text{ cm}^{-3}$  and  $T = 500$  K for the collisional de-excitation rate, there is a balance between these processes for a radiation field of  $\chi \sim 5 \times 10^3$ , which gives an expected lower limit on the radiation field above which H<sub>2</sub> vibrational excitation is expected to be efficient that it can drive the formation of CH<sup>+</sup> and SH<sup>+</sup>. Even though neglecting dissociation introduces an additional ~10% error, this calculation shows that for the radiation field in the Orion Bar ( $1 - 4 \times 10^4$  in Draine units), there is a large fraction of vibrationally excited H<sub>2</sub> to react with C<sup>+</sup> and form CH<sup>+</sup>. This has been observed by Van der Werf et al. (1996) and Walmsley et al. (2000) and has already been noted for the formation of OH through the  $\text{O} + \text{H}_2 \rightarrow \text{OH} + \text{H}$  reaction by Goicoechea et al. (2011). In the following, we test this idea with a more accurate approach, using PDR models.

##### 4.2. CH<sup>+</sup> formation

We use the 1.4.4 version of the Meudon PDR code (Le Petit et al. 2006, Goicoechea & Le Bourlot 2007, Le Bourlot et al. 2012) to model the observed CH<sup>+</sup> line intensities. This version includes the Langmuir-Hinshelwood and Eley-Rideal mechanisms to describe the formation of H<sub>2</sub> on grain surfaces. The chemical

pumping effect of destruction and formation on CH<sup>+</sup> level populations is taken into account in addition to collisional excitation and de-excitation in the Meudon code (e.g. Gonzalez Garcia et al. 2008). The Meudon code treats CH<sup>+</sup> formation as described in Agundez et al. (2010):



In reaction 1, H<sub>2</sub> rotational levels up to  $J=7$  are used, which has an energy  $E_7=4586.4$  K which is close to the activation barrier of the  $\text{H}_2 + \text{C}^+ \rightarrow \text{CH}^+ + \text{H}$  reaction. We take into account the  $v = 1$  vibrational level only as its energy (~5987 K) is enough to overcome the activation barrier of the CH<sup>+</sup> formation reaction. The formation rates are  $k_1 = 1.58 \times 10^{-10} \exp(-[4827 - E_j/k]/T)$  based on Gerlich et al. (1987) and  $k_2 = 1.6 \times 10^{-9}$  (Hierl et al. 1997).

We use isobaric models for typical conditions for the Orion Bar: pressures in the range between  $5 \times 10^7 \text{ cm}^{-3} \text{ K}$ , corresponding to  $T_{\text{kin}} \sim 500$  K (Radex models) and  $n \sim 10^5 \text{ cm}^{-3}$ , and  $2 \times 10^8 \text{ cm}^{-3} \text{ K}$ , corresponding to  $T_{\text{kin}} \sim 1000$  K (Radex models) and  $n \sim 2 \times 10^5 \text{ cm}^{-3}$ , a typical interclump medium density (e.g. Simon et al. 1997) and a radiation field on the side where the cloud is illuminated from in the range between  $\chi_{\text{front}}=10^4$  and  $3 \times 10^4$  in Draine units (Draine 1978). We run the models up to a depth equivalent to a visual extinction of  $A_V \sim 10$  mag. At the back side of the cloud (at  $A_V \sim 10$  mag), we use a radiation field 1000 times below that on the front:  $\chi_{\text{back}} = \chi_{\text{front}}/1000$ . We adopt a cosmic-ray primary ionization rate of  $\zeta = 2 \times 10^{-16} \text{ s}^{-1}$  per H<sub>2</sub> molecule suitable for the dense ISM (Hollenbach et al. 2012).

Figure 9 shows the results of a model for a pressure of  $10^8 \text{ cm}^{-3} \text{ K}$  and a radiation field of  $\chi_{\text{front}}=1 \times 10^4$ , consistent with the radiation field near the ionization front of the Orion Bar. An inclination of  $60^\circ$  was used to extract the line intensities, due to uncertainties in the computation of the line intensities in a 1D model above this value (Gonzalez Garcia et al. 2008). This is reasonably close to a model with  $75^\circ$  inclination suggested to explain the geometry of the Bar (e.g. Melnick et al. 2012). This model reproduces the observed CH<sup>+</sup> line intensities within a factor of 2 for the  $J=1-0$  transition, and with an accuracy of 20% for the other transitions. Our Radex calculations show the possible importance of electron collisions in the excitation of CH<sup>+</sup>. Therefore, to probe the effect of electron collisions on the excitation of CH<sup>+</sup>, we implemented CH<sup>+</sup>-e<sup>-</sup> collisions in the Meudon code. The models for  $P=10^8 \text{ cm}^{-3} \text{ K}$  and  $\chi = 10^4$  are shown on Figure 9. Including electrons in the excitation of CH<sup>+</sup>, the model reproduces the observed line intensities with an accuracy of ~30%. Including electron collisions affects mostly the two lowest- $J$  transitions. The predicted intensity of the  $J = 1 - 0$  transition increases by ~22%, and the intensity of the  $J = 2 - 1$  transition increases by ~18% after including electron collisions.

The CH<sup>+</sup> abundance profile corresponding to this model is shown on Figure 10 together with the gas temperature in the region where CH<sup>+</sup> abundances peak. The model predicts CH<sup>+</sup> to form near the surface of the PDR ( $A_V < 1$ ) at high ( $T \sim 500 - 1000$  K) temperatures, consistent with the predictions by Agundez et al. (2010) and with our Radex calculations. Though the best fitting models predict abundances to peak near the surface of the cloud at low  $A_V$ , the PACS observations of excited CH<sup>+</sup> used in this paper show a spatial extension along the area covered by PACS ( $47'' \times 47''$ ), as shown on Fig. 1. SPIRE observations of the  $J = 1 - 0$  transition (Naylor et al.

2010, Habart et al. 2010) show extended  $\text{CH}^+$  emission over a  $\sim 200'' \times 200''$  region centered on the  $\alpha_{J2000} = 05^{\text{h}}35^{\text{m}}22.83^{\text{s}}$ ,  $\delta_{J2000} = -05^{\circ}24'57.67''$  position.  $\text{CH}^+$   $J = 1 - 0$  emission mapped with HIFI was found to be extended over a large region covering the OMC-1 cloud (Goicoechea et al., in prep.). One possibility is that the known clumpiness of the Orion Bar is extended over a large volume and creates multiple PDR surfaces. Alternative explanation is that the extended  $\text{CH}^+$  emission seen toward the region is the result of a not completely edge-on PDR, that is tilted to the line of sight. Models with lower pressures under-predict the observed line intensities. For example, a model with a pressure of  $5 \times 10^7 \text{ K cm}^{-3}$  under-predicts the line intensities with a factor of  $\sim 4$ .

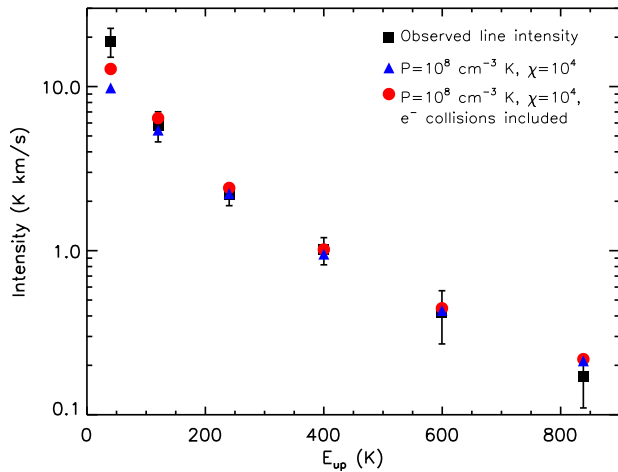


**Fig. 9.**  $\text{CH}^+$  line intensities as a function of  $E_u$  - comparison between the observed line intensities and the predictions of an isobaric PDR model with a pressure of  $10^8 \text{ cm}^{-3} \text{ K}$  for a radiation field of  $\chi = 10^4$ .

#### 4.3. $\text{SH}^+$ formation

$\text{SH}^+$  forms via a similar reaction as  $\text{CH}^+$ , however, with an endothermicity about twice as high,  $\Delta E = 9860 \text{ K}$ . Since state-to-state formation rates are not available for the  $\text{H}_2 + \text{S}^+ \rightarrow \text{SH}^+ + \text{H}$  reaction, we use the rates of the  $\text{H}_2 + \text{C}^+ \rightarrow \text{CH}^+ + \text{H}$  reaction as an approximation, taking into account  $\text{H}_2$  rotational levels up to  $E_{11} = 10261.8 \text{ K}$  and  $\text{H}_2$  in the  $v=1$  state up to  $E = 10341.5 \text{ K}$ . This is a reasonable assumption, since the total rates of the reactions for  $\text{CH}^+$  and  $\text{SH}^+$  formation via  $\text{C}^+ + \text{H}_2$  and  $\text{S}^+ + \text{H}_2$  are of the same order of magnitude (Woodall et al. 2007). To account for the higher activation barrier, we use  $k_{1,\text{mod}} = 1.58 \times 10^{-10} \exp(-[9860 - E_j/k]/T)$ . We use the 1.4.4 version of the Meudon code (Le Petit et al. 2006, Goicoechea & Le Bourlot 2007, Le Bourlot et al. 2012), where we introduce  $\text{SH}^+$  formation as described above and use scaled radiative rates (J. Black, priv. comm.) and electron-impact collisions calculated in the Coulomb-Born approximation (J. Black, priv. comm.) for the excitation of  $\text{SH}^+$ .

With these assumptions, our best fit Meudon PDR model for  $\text{CH}^+$  ( $P = 10^8 \text{ cm}^{-3} \text{ K}$ ,  $\chi = 10^4$ ) underpredicts the absolute intensities of the observed  $\text{SH}^+$  transitions by a factor of  $\sim 3.5$  for the  $F = 5/2 \rightarrow 3/2$  and  $F = 3/2 \rightarrow 1/2$  transitions and by a

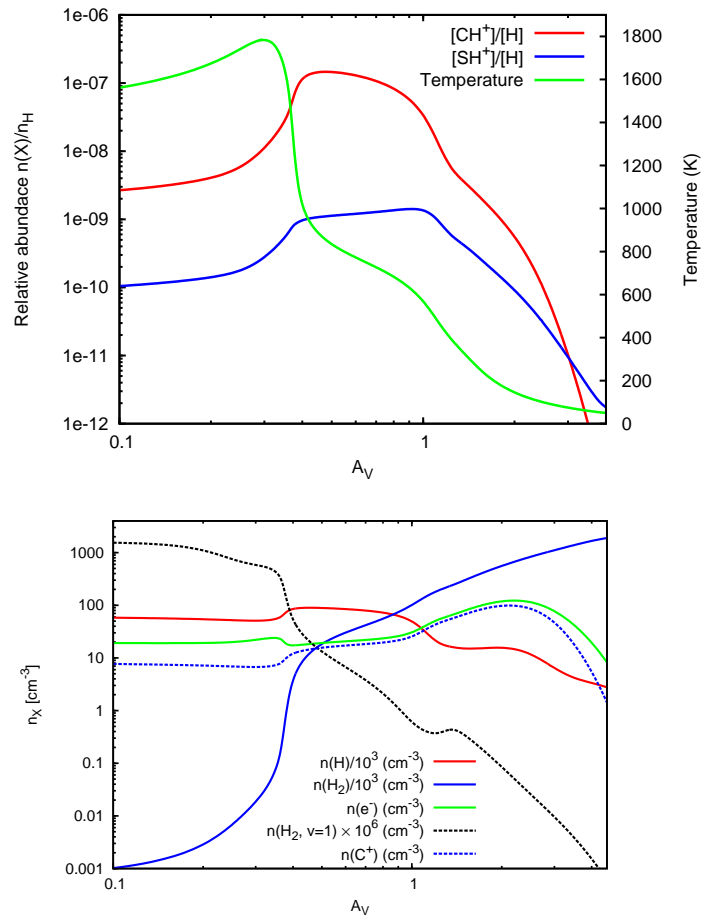
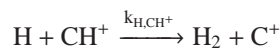


**Fig. 10.** *Top panel:*  $\text{CH}^+$  and  $\text{SH}^+$  abundances and the gas kinetic temperature as a function of  $A_V$  for a pressure of  $P = 10^8 \text{ cm}^{-3} \text{ K}$  and  $\chi = 10^4$ . *Bottom panel:*  $\text{H}$ ,  $\text{H}_2$ ,  $\text{H}_2 (v=1)$ ,  $\text{e}^-$  and  $\text{C}^+$  densities.

factor of 6.5 for the  $F = 3/2 \rightarrow 3/2$  transition. Due to the uncertainty in the formation rates, this agreement may be reasonable and suggest that similar to  $\text{CH}^+$ ,  $\text{SH}^+$  can also be formed via  $\text{H}_2$  vibrational excitation in warm and dense PDRs. It may also suggest that  $\text{SH}^+$  originates in a higher-pressure medium compared to  $\text{CH}^+$ , which would explain the difference in the observed linewidths. The  $\text{SH}^+$  abundances corresponding to this model are shown on Fig. 10.  $\text{SH}^+$  abundances, similar to  $\text{CH}^+$  abundances, peak near the surface of the cloud, at  $A_V \sim 1$  and below at high (500-1000 K) temperatures. The  $\text{SH}^+/\text{CH}^+$  abundance ratio in this region is between 0.01-0.1. This however is a lower limit on the  $\text{SH}^+/\text{CH}^+$  abundance ratio, since our model under-estimates the  $\text{SH}^+$  line intensities.

#### 5. The destruction of $\text{CH}^+$ and $\text{SH}^+$

Figure 11 shows the abundance ratio of  $\text{CH}^+$  and  $\text{SH}^+$  predicted by our best fit model in the region where  $\text{CH}^+$  and  $\text{SH}^+$  abundances peak. To understand these abundance ratios, it is essential to study the destruction of  $\text{CH}^+$  and  $\text{SH}^+$ .  $\text{CH}^+$  destruction can follow four main paths in the probed temperature and density regime:





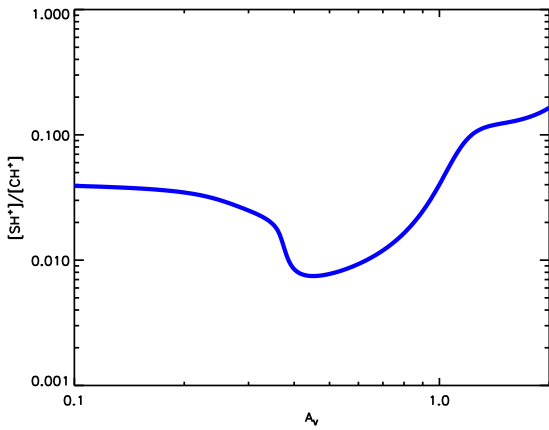
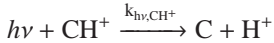
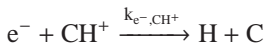
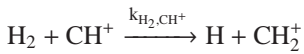
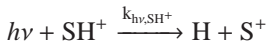
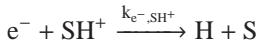
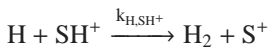


**Fig. 11.** The abundance ratios of CH<sup>+</sup> and SH<sup>+</sup> in our best fit model ( $\chi = 10^4$ ,  $P = 10^8$  cm<sup>-3</sup> K) in the warm surface region ( $A_V < 2$ ) as a function of depth into the cloud.



Unlike CH<sup>+</sup>, SH<sup>+</sup> does not react with H<sub>2</sub> at the given physical conditions, as the reaction rate is orders of magnitude lower than that of reactions with electrons and H. Therefore the most important destruction paths are photodissociation as well as chemical reactions with H and electrons:



The chemical reaction rates for these reactions are based on Woodall et al. (2007) and are summarized in Table 3.

**Table 3.** Rates corresponding to the main destruction paths of CH<sup>+</sup> and SH<sup>+</sup>, based on (Woodall et al. 2007).

Reaction	Rate (cm <sup>3</sup> s <sup>-1</sup> )	Temperature regime (K)
$k_{\text{H}, \text{CH}^+}$	$7.5 \times 10^{-10}$	10 – 41000
$k_{\text{H}_2, \text{CH}^+}$	$1.2 \times 10^{-9}$	10 – 41000
$k_{\text{e}^-, \text{CH}^+}$	$1.5 \times 10^{-7} \times (T/300)^{-0.42}$	10 – 300
$k_{\text{hv}, \text{CH}^+}$	$2.50 \times 10^{-10} \exp(-2.5/T)$	10 – 41000
$k_{\text{H}, \text{SH}^+}$	$1.10 \times 10^{-10}$	10 – 41000
$k_{\text{e}^-, \text{SH}^+}$	$2.0 \times 10^{-7} \times (T/300)^{-0.5}$	10 – 300
$k_{\text{hv}, \text{SH}^+}$	$3.00 \times 10^{-10} \exp(-1.8/T)$	10 – 41000

At a depth equivalent to a visual extinction of  $A_V \sim 0.5$  - which is in the region where the CH<sup>+</sup> and SH<sup>+</sup> abundances peak - at a temperature of  $\sim 830$  K, most CH<sup>+</sup> (73.2%) is destroyed via collisions with H, while 24.3% is destroyed via collisions with H<sub>2</sub> and 2.1% is destroyed via collisions with electrons. Photodissociation is negligible in this regime, since it is responsible for 0.4% of the destructions of CH<sup>+</sup>. Deeper in the cloud, at a depth equivalent with  $A_V \sim 1$ , at a gas temperature of  $\sim 570$  K most CH<sup>+</sup> (74.9%) is destroyed by collisions with H<sub>2</sub>, while small

fractions of CH<sup>+</sup> are destroyed via collisions with H (22.8%), electrons (2.2%) and photodissociation (0.6%).

At a depth of  $A_V \sim 0.5$ , most SH<sup>+</sup> ( $\sim 77.2\%$ ) is destroyed via reactions with H and a smaller fraction is destroyed via reactions with electrons ( $\sim 18.2\%$ ) and photodissociation ( $\sim 4.4\%$ ). At a depth corresponding to  $A_V \sim 1$ , SH<sup>+</sup> is almost equally destroyed by reactions with H ( $\sim 53.3\%$ ) and electrons ( $\sim 43.7\%$ ). A smaller fraction of SH<sup>+</sup> is destroyed via photodissociation ( $\sim 2.4\%$ ).

At  $A_V \sim 1$  and deeper, the SH<sup>+</sup> and CH<sup>+</sup> abundance ratio becomes higher than 0.1. Deeper than  $A_V \sim 1$  CH<sup>+</sup> abundances decrease more rapidly than SH<sup>+</sup> abundances. The [SH<sup>+</sup>]/[CH<sup>+</sup>] abundance ratio varies in the range between 0.01 (at  $A_V \sim 0.2$ ) and  $>0.1$  ( $A_V \sim 1$ ) and indicate that the destruction of CH<sup>+</sup> becomes more efficient as a function of the depth into the cloud where H<sub>2</sub> takes over as the most important destruction partner, while with the decrease of atomic hydrogen density SH<sup>+</sup> becomes more abundant due to electrons being a less efficient destruction partner. While in diffuse clouds the abundance ratios of [SH<sup>+</sup>]/[CH<sup>+</sup>] trace the importance of shocks (e.g. Menten et al. 2011) as well as properties of turbulent dissipation regions (e.g. Godard et al. 2012), in clouds exposed to high UV irradiation these abundances are sensitive to the abundance ratios of H, H<sub>2</sub> and electrons as a function of depth into the cloud, that are determined by the radiation field strength of the irradiation source.

## 6. Discussion

We have analyzed six rotational transitions of CH<sup>+</sup> and three transitions of SH<sup>+</sup> and reported the first detection of the  $J = 5-4$  transition of CF<sup>+</sup>. We have shown that electron collisions affect the excitation of SH<sup>+</sup> and CH<sup>+</sup>, especially the lowest- $J$  transitions. We have also shown the importance of taking reactive collisions into account in the case of CH<sup>+</sup> excitation. We have confirmed, both by an analytic approximation and more detailed PDR modeling, that CH<sup>+</sup> formation is driven by H<sub>2</sub> vibrational excitation, unlike in the case of diffuse environments with lower UV radiation fields. SH<sup>+</sup> is also likely to form via H<sub>2</sub> vibrational excitation, although the lack of information on the exact state-to-state formation rates introduces an extra uncertainty in the models.

### 6.1. The formation of CH<sup>+</sup> and SH<sup>+</sup>

A large fraction of vibrationally excited H<sub>2</sub> has been detected in the Orion Bar before the launch of Herschel (Van der Werf et al. (1996), Walmsley et al. (2000)), already indicating an importance in the chemistry of species that react with H<sub>2</sub>. Using Herschel, CH<sup>+</sup> has been detected in the Orion Bar by Naylor et al. (2010) and Habart et al. (2010), based on SPIRE maps of the 1-0 transition. These observations show extended CH<sup>+</sup> 1-0 emission in the Orion Bar as well as in the OMC-1 cloud (Naylor et al. 2010, Morris, P.; priv. comm., Goicoechea, J.; priv. comm.). Naylor et al. (2010) argue that the large spatial extent of CH<sup>+</sup>, into regions of low  $A_V$ , suggests the importance of the formation via H<sub>2</sub> vibrational excitation. Our observations extend these studies, since the additional observed transitions up to  $J=6-5$  provide further evidence on the importance of the formation via vibrationally excited H<sub>2</sub>. An origin of CH<sup>+</sup> in the warm surface regions of the PDR is further confirmed by Goicoechea et al. (2011), who find a spatial correlation between excited OH  $^2\Pi_{3/2} J = 7/2^- \rightarrow 5/2^+$  ( $\sim 84.6 \mu\text{m}$ , observed with PACS) and CH<sup>+</sup> 3-2 emission, and that OH originates in the surface region

( $A_V < 1$ ) of a high pressure gas component ( $10^8 - 10^9$  K  $\text{cm}^{-3}$ ) component. The formation and excitation of  $\text{CH}^+$  in the Orion Bar is somewhat similar to that in the envelope of the high-mass protostar AFGL 2591, as it can be explained to originate in the FUV-irradiated outflow-walls (Bruderer et al. 2010). Another region where  $\text{CH}^+$  formation is driven by the strong FUV radiation field and can be explained by  $\text{H}_2$  vibrational excitation is the protoplanetary disc HD 100546 (Thi et al. 2011), where  $\text{CH}^+$  emission mostly originates in the outer disc and the disc surface in warm gas ( $T_{\text{gas}} > 400$  K).

Other explanations for the formation of  $\text{CH}^+$  applicable to the diffuse ISM include shocks (e.g. Pineau des Forêts et al. (1986)). Tielens et al. (1993) have investigated, that shocks do not contribute to the chemistry of the Orion Bar, therefore, we consider this scenario unlikely. Another scenario for  $\text{CH}^+$  formation, that has been successful in reproducing  $\text{CH}^+$  abundances for the diffuse interstellar medium is the dissipation of turbulence (Godard et al. 2009, 2012). Though the  $\text{CH}^+$  1-0 and 2-1 transitions have broader line widths than most dense gas tracers in the Orion Bar, most of the lines detected in the Orion Bar are narrow (2-3  $\text{km s}^{-1}$ ), therefore we find it unlikely that turbulence plays a role in the chemistry of species detected in the Orion Bar.

Unlike  $\text{CH}^+$ ,  $\text{SH}^+$  has not been observed in a large variety of regions yet since its recent discovery in absorption toward Sagittarius B2 (Menten et al. 2011). A recent study by Godard et al. (2012) probes  $\text{CH}^+$  and  $\text{SH}^+$  in absorption in the diffuse interstellar medium toward high-mass star-forming regions, suggesting a common origin for the formation and excitation of these ions, based on their observed linewidth-distributions and on comparison with MHD shock models. However, in the diffuse ISM,  $\text{SH}^+$  and  $\text{CH}^+$  abundances are influenced by the dissipation of turbulence.  $\text{SH}^+$  has also been detected in emission in the high-mass star-forming region W3 IRS5 (Benz et al. 2010), which represents a region with physical conditions comparable to the Orion Bar, where the UV-radiation of the embedded protostars drives the chemistry of  $\text{SH}^+$ .

## 6.2. $\text{CH}^+$ and $\text{SH}^+$ as tracers of the warm PDR surface

Though  $\text{CH}^+$  and  $\text{SH}^+$  most likely form via the same process and originate in the warm surface region of the PDR, a significant difference between  $\text{CH}^+$  and  $\text{SH}^+$  emission is suggested by the difference in the observed line-widths. While the observed line width of  $\text{SH}^+$  ( $\Delta v \sim 3$   $\text{km s}^{-1}$ ) is closer to that of dense gas tracers ( $\Delta v \sim 2-3$   $\text{km s}^{-1}$ ), the width of the  $\text{CH}^+$   $J = 1 - 0$  and 2-1 transitions ( $\Delta v \sim 5$   $\text{km s}^{-1}$ ) is similar to that of HF ( $\Delta v \sim 4.9$   $\text{km s}^{-1}$ , Van der Tak et al. 2012) and  $\text{C}^+$  ( $\Delta v \sim 3.8$   $\text{km s}^{-1}$ ) a tracer of the interclump medium. The C91 $\alpha$  carbon recombination line was observed with the VLA with a width of 2-2.5  $\text{km s}^{-1}$  (Wyrowski et al. 1997). It was found to match the  $\text{H}_2$  [1-0 S(1)] distribution (Van der Werf et al. 1996), and its radial velocity to be consistent with that of  $\text{H}_2$  pure rotational lines  $\text{H}_2$   $v=0-0$  S(1), S(2) and S(4) (Allers et al. 2005). The  $^{13}\text{C}^+$  lines have a slightly larger width of 2.5-2.8  $\text{km s}^{-1}$ , compared to that of the C91 $\alpha$  line. The larger width of the [CII] 158  $\mu\text{m}$  line compared to the  $^{13}\text{C}^+$  lines can be a result of optical depth broadening of the  $\text{C}^+$  line (with an optical depth of 2-3). However, the  $\text{C}^+$  line is broader also near the edge of the Bar, where the column density of material is lower, and also the line optical depths. In addition, the recombination line intensity is sensitive to the square of the electron density, while the fine structure line is sensitive to the local density only. Therefore the difference in line profile outside opacity broadening may also be related to gradients in the

beam and along the line of sight, with the denser material having a lower velocity dispersion.

This possible difference in the properties of the emitting regions is further indicated by our Radex models (Section 3.2). These models reproduce the observed  $\text{CH}^+$  line intensities with a temperature of  $T = 500 - 1000$  K and a density of  $n \sim 10^5$   $\text{cm}^{-3}$ , but suggest a higher density component to explain  $\text{SH}^+$  emission,  $T \sim 200$  K,  $n \sim 10^6$   $\text{cm}^{-3}$ , which is consistent with the properties of warm and dense condensations suggested to explain the origin of excited OH (Goicoechea et al. 2011) and high- $J$  CO line emission (Joblin et al. 2012, in prep.). In this case, thermal line broadening may contribute to the difference between the widths of the  $\text{CH}^+$  and  $\text{SH}^+$  lines. The expected contribution of thermal line broadening for  $\text{CH}^+$  is  $\Delta v = 2 \sqrt{2 \ln 2} \sqrt{\frac{kT}{m}} = 1.3$   $\text{km s}^{-1}$  for  $T_{\text{kin}} = 500$  K and  $\Delta v = 1.8$   $\text{km s}^{-1}$  for  $T_{\text{kin}} = 1000$  K. The contribution of thermal line broadening for  $\text{SH}^+$  for  $T_{\text{kin}} = 200$  K is  $\Delta v = 0.6$   $\text{km s}^{-1}$ .

As an alternative explanation of the large observed line width of  $\text{CH}^+$ , formation pumping may play a role in the broadening of  $\text{CH}^+$ . As explained in section 3.2,  $\text{CH}^+$  formation results in an excess energy equivalent to 5360 K. This energy may be redistributed and go into kinetic motions. If the 5360 K excess energy goes into excess translational energy of the nascent  $\text{CH}^+$ , and if this is identified as an ionic kinetic temperature upon formation, then the corresponding FWHM of Doppler motions is 4.4  $\text{km s}^{-1}$ .

The difference between the widths of  $\text{CH}^+$  and  $\text{SH}^+$  may not originate in different excitation conditions, but in the difference in the chemistry of these ions. After its formation,  $\text{CH}^+$  rapidly reacts with H and  $\text{H}_2$ , therefore it is likely, that its translational motions never become thermalized. In this case, the large velocity dispersion in  $\text{CH}^+$  partially reflects the conditions of its formation.  $\text{SH}^+$  on the other hand does not react rapidly with H (and  $\text{H}_2$ ), so that it is destroyed less rapidly by recombination with electrons. Therefore,  $\text{SH}^+$  can become thermalized translationally during its chemical lifetime. Therefore, while  $\text{SH}^+$  traces the density and the temperature of the emitting region,  $\text{CH}^+$  is more sensitive to the details of its formation process.

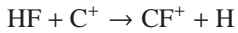
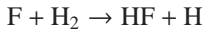
Another interpretation of the broadening of  $\text{CH}^+$  and other molecules could be that they originate in flows created by photo-evaporating clumps (e.g. Gorti & Hollenbach 2002, Mackey & Lim 2010). However, our observed data don't completely support this assumption. If the FWHM of ions and other molecules detected at the same position had a contribution by the evaporating flow, we would expect  $\text{C}^+$  and  $\text{CH}^+$  to have a similar flow velocity, as the momentum transfer from  $\text{H}_2$  in the  $\text{H}_2^+ + \text{C}^+$  reaction is small. Based on our HIFI observations of the  $\text{CO}^+$  peak, this does not apply, as  $\text{FWHM}(\text{C}^+) \sim 3.8$   $\text{km s}^{-1}$  and  $\text{FWHM}(\text{CH}^+) \sim 5$   $\text{km s}^{-1}$ .

The difference in the width of reactive ions tracing the warm surface region of the PDR is a key part of understanding the chemistry of these ions. Future observations of the spatial distribution of  $\text{SH}^+$  will help to distinguish between these explanations.

## 6.3. An extension of the ' $\text{CF}^+$ ladder' in the Orion Bar

Unlike  $\text{CH}^+$  and  $\text{SH}^+$ ,  $\text{CF}^+$  does not directly form via collisions with  $\text{H}_2$ . The reaction between fluorine and  $\text{H}_2$  is followed by a reaction between  $\text{C}^+$  and HF, where HF is the dominant reservoir of fluorine and has previously been detected in emission in the

Orion Bar by Van der Tak et al. (2012):



CF<sup>+</sup> is the second most important fluorine reservoir and accounts for ~1% of the gas-phase fluorine abundance. However, CF<sup>+</sup> has so far only been detected in two sources. The 2-1 and 1-0 rotational transitions have been recently detected with a spatially extended emission toward the PDR in the Horsehead nebula (Guzmán et al. 2012). The first detection of CF<sup>+</sup> was toward the Orion Bar (Neufeld et al. 2006), showing spatially extended emission in the 1-0, 2-1 and 3-2 rotational transitions. Our observations extend the observed CF<sup>+</sup> transitions toward the Orion Bar up to the 5-4 transition and since the line intensity is consistent with the previously observed transitions, this work gives a further confirmation on the simple CF<sup>+</sup> chemistry tracing the surface layers exposed to UV irradiation.

## 7. Conclusions and outlook

We have analyzed six rotational transitions of CH<sup>+</sup> and three transitions of SH<sup>+</sup> and reported the first detection of the 5-4 transition of CF<sup>+</sup>. Our main conclusions are the following:

- We have detected CH<sup>+</sup> up to the 6-5 transition. The 2-1 and 1-0 transitions are spectrally resolved and show significantly broader lines ( $\Delta v \sim 5 \text{ km s}^{-1}$ ) than most dense gas tracers in the Orion Bar. SH<sup>+</sup> on the other hand shows significantly narrower lines than CH<sup>+</sup> ( $\Delta v \sim 3 \text{ km s}^{-1}$ ). Explanations of this difference include that they originate in a different density (and temperature) component. Alternatively, due to its reactivity, CH<sup>+</sup> never becomes thermalized, therefore, its observed properties rather trace the formation process than the properties of the emitting region, unlike for SH<sup>+</sup>. Information on the spatial distribution of SH<sup>+</sup> is needed to resolve this puzzle.
- Inelastic collisions with H<sub>2</sub> and electrons both affect the excitation of CH<sup>+</sup> and SH<sup>+</sup>, similar to the case of HF (Van der Tak et al. 2012). Reactive collisions are important in the excitation of CH<sup>+</sup>, but have less effect in the case of SH<sup>+</sup>.
- Comparing the observed CH<sup>+</sup> intensities to predictions of PDR models for typical conditions in the Orion Bar, we confirm that CH<sup>+</sup> forms via reactions with vibrationally excited H<sub>2</sub>, as predicted by Agúndez et al. (2010). Our PDR models also show that CH<sup>+</sup> forms in the warm ( $T \sim 500 - 1000 \text{ K}$ ) surface region of the PDR at high ( $\sim 10^8 \text{ cm}^{-3}$ ) pressures.
- SH<sup>+</sup> is also likely to form via H<sub>2</sub> vibrational excitation, assuming that the formation rates are similar to that of CH<sup>+</sup>. SH<sup>+</sup> is also a tracer of the warm surface regions of the PDR.

In the future, higher-resolution follow-up observations of a larger region in the Orion Bar will give more insight into the excitation conditions of SH<sup>+</sup>. Probing CH<sup>+</sup> and SH<sup>+</sup> formation in PDRs with a range of parameters, such as different radiation fields would help to deepen our understanding of the chemistry of these ions in regions exposed to UV irradiation.

## References

- Agúndez, M., Goicoechea, J. R., Cernicharo, J., et al. 2010, ApJ, 713, 662  
 Allers, K. N., Jaffe, D. T., Lacy, J. H., Draine, B. T., & Richter, M. J. 2005, ApJ, 630, 368  
 Benz, A. O., Bruderer, S., van Dishoeck, E. F., et al. 2010, A&A, 521, 35  
 Bergin, E. A., Phillips, T. G., Comito, C., et al. 2010, A&A, 521, L20+

- Bruderer, S., Benz, A. O., van Dishoeck, E. F., et al. 2010, A&A, 521, L44  
 Coutens, A.; Vastel, C.; Caux, E. et al. 2012, A&A 539, 132  
 Douglas, A. E., & Herzberg, G. 1941, ApJ, 94, 381  
 Draine, B. T. 1978, ApJS, 36, 595  
 Falgarone, E., Godard, B., Cernicharo, J., et al. 2010a, A&A, 521, 15  
 Falgarone, E., Ossenkopf, V., Gerin, M., et al. 2010b, A&A, 518, 118  
 Fuente, A.; Rodríguez-Franco, A.; García-Burillo, S. et al. 2003, A&A, 406, 899  
 Gerlich, D., Disch, R., & Scherbarth, S. 1987, J. Chem. Phys., 87, 350  
 Godard, B., Falgarone, E., & Pineau Des Forêts, G. 2009, A&A, 495, 847  
 Godard, B., Falgarone, E., Gerin, M., et al. 2012, A&A, 540, 87  
 Goicoechea, J. R., & Le Bourlot, J. 2007, A&A, 467, 1  
 Goicoechea, J. R., Joblin, C., Contursi, A., et al. 2011, A&A, 530, L16  
 Gonzalez Garcia, M., Le Bourlot, J., Le Petit, F. & Roueff, E. 2008, A&A 485, 127  
 Gorti, U. & Hollenbach, D. 2002, ApJ 573, 215  
 Guzmán, V.; Pety, J.; Gratier, P. et al. 2012, A&A 543, 1  
 Habart, E., Dartois, E., Abergel, A., et al. 2010, A&A, 518, L116  
 Hierl, P. M., Morris, R. A., & Viggiano, A. A. 1997, J. Chem. Phys., 106, 10145  
 Hogerheijde, M. R.; Jansen, D. J. & Van Dishoeck, E. F. 1995, A&A 294, 792  
 Hollenbach, D.; Kaufman, M. J.; Neufeld, D.; Wolfire, M.; Goicoechea, J. R. 2012, ApJ 754, 105  
 Le Bourlot, J., Le Petit, F., Pinto, C., Roueff, E., & Roy, F. 2012, A&A, 541, A76  
 Le Petit, F., Nehmé, C., Le Bourlot, J., & Roueff, E. 2006, ApJS, 164, 506  
 Lim, A. J.; Rabadán, I. & Tennyson, J. 1999, MNRAS 306, 473  
 Lis, D. C., Serabyn, E., Keene, J., et al. 1998, ApJ, 509, 299  
 Lis, D. C., & Schilke, P. 2003, ApJ, 597, 145  
 Mackey & Lim 2010, MNRAS 403, 714  
 Magnani, L. & Salzer, J. J. 1989, AJ, 98, 926  
 Magnani, L. & Salzer, J. J. 1991, AJ, 101, 1429  
 Melnick, G.; Tolls, V.; Goldsmith, P. et al. 2012, ApJ, 752, 26  
 Menten, K. M., Reid, M. J., Forbrich, J., & Brunthaler, A. 2007, A&A, 474, 515  
 Menten, K. M., Wyrowski, F., Belloche, A., et al. 2011, A&A, 525, A77+  
 Millar, T. J. & Hobbs, L. M. 1988, MNRAS, 231, 953  
 Müller, H. S. P., Schöder, F., Stutzki, J., & Winnewisser, G. 2005, J. Mol. Struct., 742, 215  
 Müller, H. S. P. 2010, A&A 514, L6  
 Naylor, D. A., Dartois, E., Habart, E., et al. 2010, A&A, 518, L117  
 Neufeld, D. A., Schilke, P., Menten, K. M., et al. 2006, A&A, 454, L37  
 Ossenkopf, V., Röllig, M., Neufeld, D. A. et al. 2012, A&A, in press (arXiv:1211.3359)  
 Ott, S., Science Centre, H., & Space Agency, E. 2010, ArXiv e-prints  
 Pineau des Forêts G., Flower, D. R., Hartquist, T. W., & Dalgarno, A. 1986, MNRAS, 220, 801  
 Poglitsch, A., Waelkens, C., Geis, N., et al. 2010, A&A, 518, L2  
 Roelfsema, P., Helmich, F., Teyssier, D., et al. 2012, A&A, 537, 17  
 Röllig, M., Ossenkopf, V., Jeyakumar, S., Stutzki, J., & Sternberg, A. 2006, A&A, 451, 917  
 Schöier, F. L.; Van der Tak, F. F. S.; Van Dishoeck, E. F. and Black, J. H. 2005, A&A 432, 369  
 Simon, R., Stutzki, J., Sternberg, A., & Winnewisser, G. 1997, A&A, 327, 9  
 Sternberg & Dalgarno 1995, ApJS, 99, 565  
 Störzer, H., Stutzki, J., & Sternberg, A. 1995, A&A, 296, L9  
 Thi, W.-F., Ménard, F., Meeus, G., et al. 2011, A&A, 530, L2  
 Tielens, A. G. G. M. et al. 1993, Science 262, 86  
 Turpin, F.; Stoecklin, T.; Voronin, A. 2010, A&A 511, 28  
 Van Dishoeck, E. F., & Black, J. H. 1986, ApJS, 62, 109  
 Van der Tak, F.F.S., Black, J.H., Schöier, F.L., Jansen, D.J., van Dishoeck, E.F., 2007, A&A 468, 627-635  
 Van der Tak, F.F.S., Ossenkopf, V., Nagy, Z. et al. 2012, A&A 537, 10  
 van der Werf, P., Stutzki, J., Sternberg, A., & Krabbe, A. 1996, A&A, 313, 633  
 Van der Wiel et al 2009, A&A 498, 161-165  
 Walmsley, C. M., Natta, A., Oliva, E., & Testi, L. 2000, A&A, 364, 301  
 Woodall, J.; Agúndez, M.; Markwick-Kemper, A. J.; Millar, T. J. 2007, A&A 466, 1197  
 Wyrowski, F.; Schilke, P.; Hofner, P. & Walmsley C. M., 1997, ApJ, 487, L171  
 Young Owl, R. C., Meixner, M. M., Wolfire, M., Tielens, A. G. G.M., & Tauber, J. 2000, ApJ, 540, 886

**Acknowledgements.** We thank the referee for the constructive suggestions that helped to improve the paper. We also thank the editor Malcolm Walmsley for additional comments. We thank Simon Bruderer for useful comments on CH<sup>+</sup> and SH<sup>+</sup> and Yunhee Choi for the help in the reduction of the HIFI data. J.R.G. is supported by a Ramón y Cajal research contract and thanks the Spanish MINECO for funding support through grants AYA2009-07304 and CSD2009-00038. Support for this work for E.A.B. was provided by NASA through an award issued by JPL/Caltech. Part of the work was supported by the *Deutsche Forschungsgemeinschaft* through grant SFB 956 C1. HIFI has been designed and built by a consortium of institutes and university departments from across Europe, Canada and the US under the leadership of SRON

Netherlands Institute for Space Research, Groningen, The Netherlands with major contributions from Germany, France and the US. Consortium members are: Canada: CSA, U. Waterloo; France: IRAP, LAB, LERMA, IRAM; Germany: KOSMA, MPIfR, MPS; Ireland, NUI Maynooth; Italy: ASI, IFSI-INAF, Arcetri-INAF; Netherlands: SRON, TUD; Poland: CAMK, CBK; Spain: Observatorio Astronomico Nacional (IGN), Centro de Astrobiología (CSIC-INTA); Sweden: Chalmers University of Technology - MC2, RSS & GARD, Onsala Space Observatory, Swedish National Space Board, Stockholm University - Stockholm Observatory; Switzerland: ETH Zürich, FHNW; USA: Caltech, JPL, NHSC. HIPE is a joint development by the Herschel Science Ground Segment Consortium, consisting of ESA, the NASA Herschel Science Center, and the HIFI, PACS and SPIRE consortia.

PACS has been developed by a consortium of institutes led by MPE (Germany) and including UVIE (Austria); KU Leuven, CSL, IMEC (Belgium); CEA, LAM (France); MPIA (Germany); INAF/IFI/OAA/OAP/OAT, LENS, SISSA (Italy); IAC (Spain).